Journal of Materials Chemistry A

ROYAL SOCIETY OF CHEMISTRY

PAPER

View Article Online
View Journal | View Issue

Cite this: J. Mater. Chem. A, 2023, 11, 16127

Ultralow loading of carbon quantum dots leading to significantly improved breakdown strength and energy density of P(VDF-TrFE-CTFE)†

Xun Jiang, Hang Luo, * Fan Wang, Xiaona Li, Haoran Xie, Yuan Liu, Guoqiang Zou, Xiaobo Ji, Hongshuai Hou * and Dou Zhang*

Received 4th May 2023
Accepted 28th June 2023

DOI: 10.1039/d3ta02642f

rsc.li/materials-a

Relaxor ferroelectric polymer P(VDF-TrFE-CTFE) is attracting increasing attention for electronic applications due to its high dielectric constant and relaxation characteristic. However, the low breakdown strength and premature saturation of polarization of this polymer have hampered its practical application severely. In this work, carbon quantum dots (CQDs) with functional groups and size of about 5 nm have been incorporated to overcome these issues. The nanocomposite with 0.1 wt% CQDs presents significantly improved breakdown strength and discharge energy density. Its breakdown strength (E_b) has been increased by 30.7% up to 340 kV mm^{-1}. Due to the Coulomb blockade effect, the electrons can be restrained in the deep traps, which is favorable for the improvement of breakdown strength. Besides, the abundant functional groups around CQDs are beneficial to form adequate hydrogen bonds, resulting in increased crystallinity and breakdown strength as well. Additionally, the discharge energy density has been improved by 41.7% up to 6.8 J cm^{-3}. The study demonstrates the effective enhancement of breakdown strength and energy density by ultralow loading of CQDs for P(VDF-TrFE-CTFE) polymer.

Introduction

Capacitors with super-high power density and fast-speed charging–discharging processes have a broad application prospect, such as wind power, rail transportation, military equipment, and electrical energy storage.[1–4] In the background of explosive development of the electronic information industry, breakthrough in key technology of capacitors is exigent for the application in new energy automobiles, intelligent terminals, and industry network.[5–8] Dielectrics with high breakdown strength (E_b) and large discharge energy density (U_d) ought to be developed urgently.

For dielectrics with dipoles inside, energy charging–discharging can be realized through the polarization–depolarization process, which can be described by a displacement hysteresis loop (the D–E curve). Based on the D–E curve, the charging energy density or U_d of the dielectrics at a specific electric field can be calculated using the formula: $U = \int E\mathrm{d}D = \int \varepsilon_0\varepsilon_r E\mathrm{d}E$, where U, E and D stand for the energy density, applied electric field, and displacement, respectively. ε_0 is the permittivity of the vacuum (8.85×10^{-12}), and ε_r is the relative permittivity (dielectric constant) of the dielectrics. Additionally, the electric field with the maximal displacement is called the dielectric breakdown strength (E_b).

In comparison with ceramic dielectrics, polymer dielectrics with greater flexibility and E_b have aroused widespread attention.[9–12] For example, the E_b at room temperature of commercial BOPP can be as high as 700 kV mm^{-1}.[13,14] However, its U_d is limited due to the low dielectric constant (~3). To overcome this problem, PVDF has been explored owing to its higher dielectric constant associated with the permanent dipoles. PVDF is a kind of crystallizable polymer and there are

State Key Laboratory of Powder Metallurgy, Central South University, Changsha 410083, Hunan Province, China. E-mail: hangluo@csu.edu.cn; hs-hou@csu.edu.cn; dzhang@csu.edu.cn

† Electronic supplementary information (ESI) available. See DOI: https://doi.org/10.1039/d3ta02642f

Dr Hongshuai Hou is a Professor of College of Chemistry and Chemical Engineering at Central South University. He received his master's degree from Tianjin University in 2013 and PhD degree from Central South University in 2016, and then worked at Central South University. His research focuses on the application of carbon dots in advanced energy materials, involving cathode/anode materials, electrolytes, and membrane materials for secondary batteries and capacitors. He has published more than 200 papers in international journals.

three main crystalline forms commonly, *i.e.* α, γ, and β phases.[15,16] In the α phase, the dipoles orient randomly and show electric neutrality, which does not help to increase the dielectric constant; dipoles in the γ phase are oriented partially, resulting in a slight increase of polarity; the dipoles in the β phase orient in the same direction generating huge polarization.[17–19] Yet, coupling among dipoles leads to larger energy loss because the energy barrier is higher for dipoles to switch back to the equilibrium state.[20] It has been discovered that the introduction of CFE or CTFE monomer into the molecular chain of PVDF can enlarge the interchain spacing and weaken the interaction of the polar dipoles.[21,22] Meanwhile, the P(VDF-TrFE-CTFE) ternary polymer possesses a high dielectric constant because of its strong polar bonds and the relaxation characteristic, attracting increasing attention in the energy storage field.[23] Nevertheless, the weak E_b associated with the poor Young's modulus and the premature saturation of the polarization lead to the low U_d, limiting its application.[3,24,25] Thus, it is a crucial task to enhance the E_b of the ternary polymer.

With regard to polymer dielectrics, the most threatening issue is the conductivity loss especially at high temperature and high electric field.[24,26] The conductivity of polymers not only leads to huge dielectric loss but also produces a large amount of heat to increase the working temperature and accelerate the breakdown process. The charge carriers to form leakage current can originate from the intrinsic polymer and the charge injection.[26] Furthermore, the electromechanical breakdown is the reason for the failure of the polymer dielectrics as well. This mechanism is related to the plastic deformation under electric fields. In summary, the main aim is to restrain the conductivity and reinforce the ternary polymer to reach higher E_b.

Efforts have been devoted to addressing this vital limitation. Liu *et al.* prepared P(VDF-TrFE-CTFE) film with E_b of 600 kV mm^{-1} and U_d of 17 J cm^{-3} *via* grafting poly(styrene-methyl methacrylate) chains onto the polymer. Zhang *et al.* introduced hydrogen bonds into P(VDF-TrFE-CTFE) chains and increased the Young's modulus of the amorphous phase, resulting in an E_b of 500 kV mm^{-1}.[27] Zhu *et al.* constructed a sandwich structure with crosslinked PVDF clamped by P(VDF-TrFE-CTFE) on the outside, and an E_b of 550 kV mm^{-1} and a U_d of 18.3 J cm^{-3} were achieved.[28] On the other hand, the modification towards polymer chains is effective but hard to conduct. Chi *et al.* prepared nanocomposite films with an E_b of 380 kV mm^{-1} and U_d of 12.93 J cm^{-3} by adding wide-bang-gap BNNs in gradient content.[29] The addition of inorganic fillers into polymers is a feasible and facile method to improve the energy storage properties. However, filler loading needs to be high enough for greater ε_r, which will cause severe aggregation and higher local electric field, leading to more charge carriers and weaker E_b.[30] Therefore, reasonable solutions need to be put forward to solve the problem.

Carbon quantum dots (CQDs) are a novel type of semiconductor quantum material, attracting a wide range of attention in fields like advanced batteries, biomedicine, photocatalysis and so on.[31–34] CQDs possess a lot of special characteristics such as functional groups, quantum effect, photoluminescence, and great biocompactivity, where the Coulomb blockade effect is the behaviour that prevents electron tunneling.[35,36] Once the particle size is reduced to a certain degree, an energy barrier can be formed owing to the strong Coulomb repulsion among electrons.[37] Consequently, electrons can be suppressed to hop under a certain threshold. As such, CQDs with quantum-scale size can provide large interfaces and thick permeators to capture the space charges potentially.[38,39] Besides, the electrons captured by traps are prone to be confined to hop due to the Coulomb blockade effect. Additionally, the abundant functional groups on its surface may avoid the aggregation issue especially when the filler content is relatively low.

In this work, a series of nanocomposite films with different CQD filler contents are prepared *via* a solution-casting method. It turns out that the E_b and the energy efficiency have been improved effectively with ultralow loading. With the addition of CQDs, the crystallinity increased due to its interface effect, which is favourable for lengthening the electric tree path and generating a depolarization electric field. The nanocomposite with a CQD content of 0.1 wt% presents better performance. The E_b has been enhanced by 30.7%, up to 340 kV mm^{-1} and the energy efficiency at 160 kV mm^{-1} is as high as 68.0%. On account of the enhancement of E_b, the maximal U_d has been improved by 41.7%, from 4.8 J cm^{-3} to 6.8 J cm^{-3} for the pristine film and the nanocomposite film at 0.1 wt% CQD loading, respectively.

Results and discussion

The high-resolution TEM images are shown in Fig. 1a and b, illustrating that the CQDs are monodisperse spherical particles with diameter near 5 nm and good crystal structure. Fig. 1c shows the great dispersity of the CQDs in ethanol solvent. The FTIR spectrum of CQDs is presented in Fig. 1d. As demonstrated, CQDs contain several types of functional groups, such as the carbon–carbon double bond (C=C), hydroxyl (–OH), and carbonyl (C=O) double bond.[40,41] The XPS spectra depicted in Fig. 1e and f correspond well with the FTIR spectrum. These functional groups can be favourable for the surface functionalization of CQDs and beneficial for their unique properties.

The CQDs possess favourable dispersion in DMF solvent, as shown in Fig. 2a and S1 (ESI†). Since CQDs are a novel semiconductor quantum material with excellent photo-luminescence, LSCM is employed to confirm the dispersibility of CQDs in nanocomposite films. As illustrated in Fig. 2c–h, yellow dots scatter uniformly on each image. Besides, the yellow in different images becomes brighter with increasing the CQDs content. In other words, the CQDs are compatible with the homogeneous P(VDF-TrFE-CTFE) ternary polymer and well dispersed in the nanocomposite films with great stability. During the synthesis of CQDs, the aldol reaction process of acetone can occur under strong alkaline conditions as well as a series of side reactions. The products, unsaturated ketone, can further polymerize, forming oligomers with extended carbon chains whose components are functional groups (C–OH, CH_2–/CH_3, and C=O). Then the oligomers may curl and intertwine to produce several nanodots. Therefore, the CQDs possess a similar

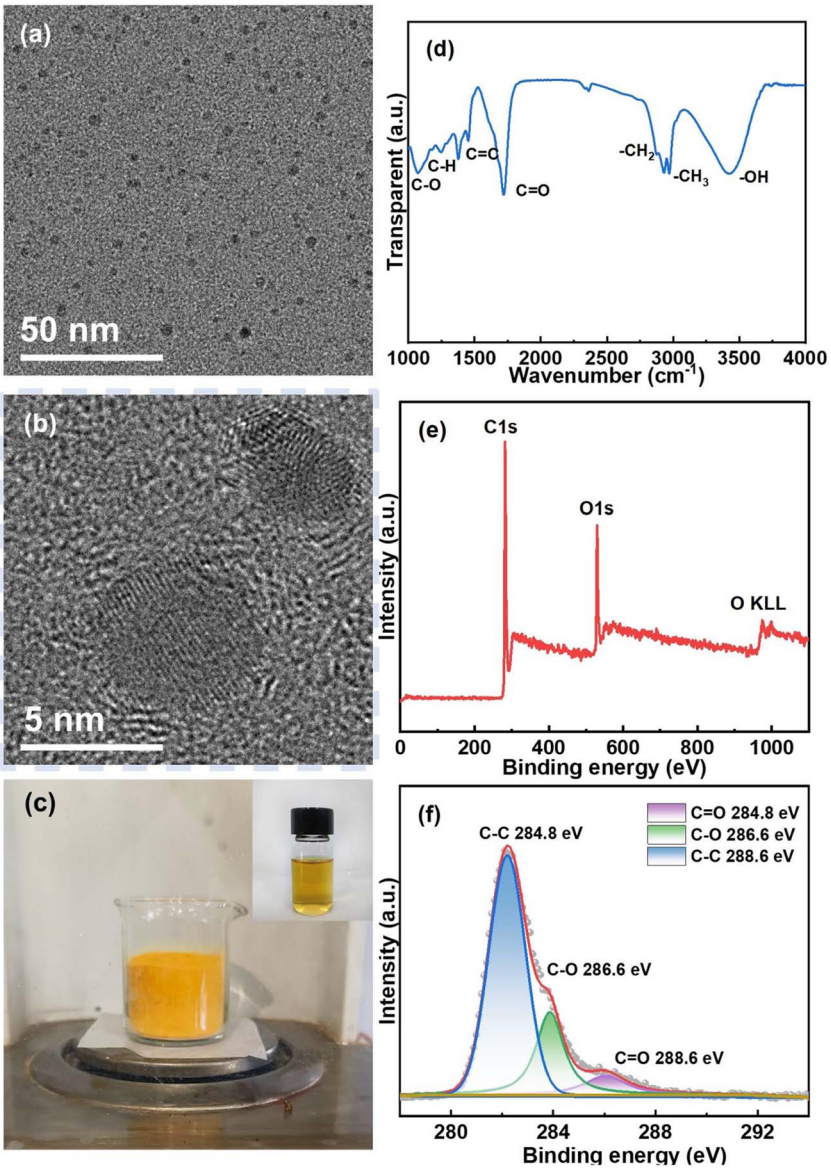

Fig. 1 (a and b) High-res TEM images. (c) Digital images of CQDs and CQDs/ethanol solution. (d) FTIR spectrum. (e) Survey XPS spectrum. (f) C 1s high-resolution XPS spectra of CQDs.

structure to the solvent and polymer matrix, accounting for their good compatibility.

Frequency dependence of dielectric permittivity under low electric field

The results of dielectric frequency spectroscopy are exhibited in Fig. 3a and b. There are five types of polarization in dielectrics, of which dipolar relaxation plays the most important role, ranging from 1 Hz to 100 MHz.[42] The dielectric constant of all nanocomposites declines monotonously with increasing frequency, which is related to the weaker dielectric response of dipoles to higher frequency. The dielectric loss presents a peak at about 10^6 Hz with frequency, which is caused by the dipole relaxation.[43] For a quantitative understanding of the influence on nanocomposites brought about by CQDs, ε_r and dielectric loss at 1 kHz of each nanocomposite are compared. As shown in Fig. 3c and d, the ε_r increases with addition of CQDs, and it changes from 29.4 to 34.3 at 0.1 wt% CQD loading. Since CQDs are a kind of spherical particle with a diameter of about 5 nm, a large specific area and interface can be generated. Space charges can accumulate in these interface and result in an increase of the permittivity.[44–46] Besides, it is notable that the dielectric loss shows very little difference among all the CQDs/P(VDF-TrFE-CTFE) nanocomposites in Fig. 3b due to ultra-low filler loading.

Weibull analysis of electric breakdown strength

The measured E_b is 260 kV mm^{-1}, 300 kV mm^{-1}, 340 kV mm^{-1}, 320 kV mm^{-1}, 280 kV mm^{-1} and 260 kV mm^{-1} for the pristine ternary polymer film and the CQDs/P(VDF-TrFE-CTFE)

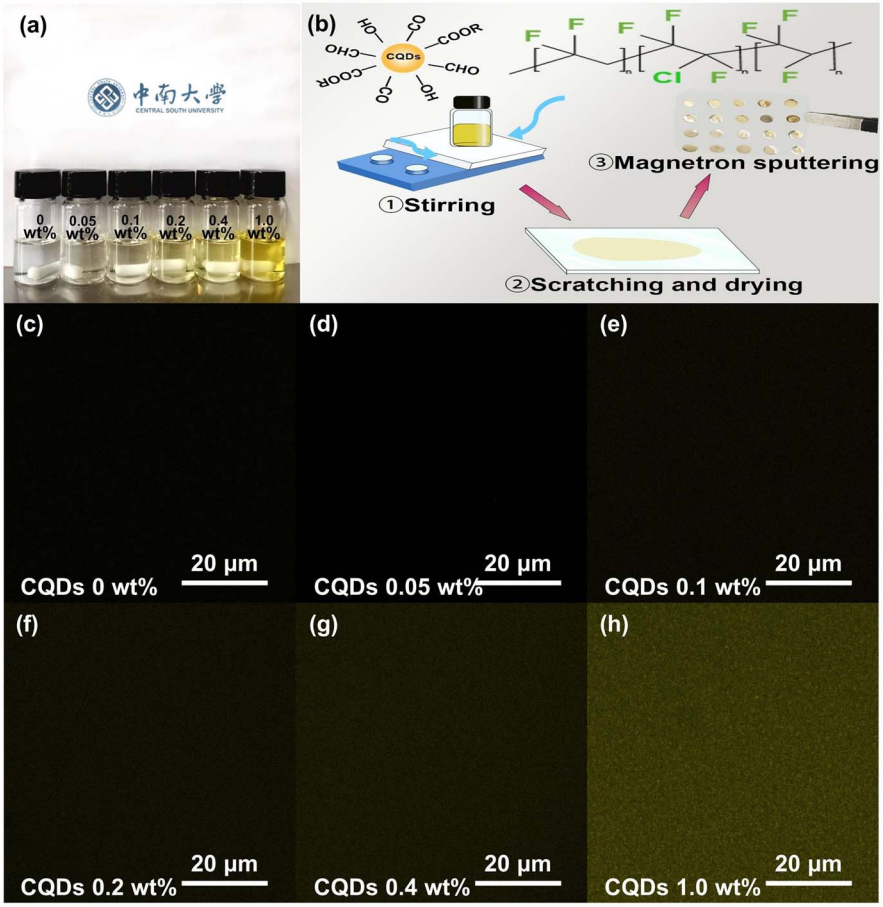

Fig. 2 (a) Digital images of CQDs/P(VDF-TrFE-CTFE) solutions with different CQD content. (b) The scheme of the nanocomposite fabrication. (c–h) The fluorescence images of the nanocomposites recorded by LSCM.

nanocomposite films with CQD content of 0.05 wt%, 0.1 wt%, 0.2 wt%, 0.4 wt% and 1.0 wt%, respectively. It is surprising to find that the E_b presents a 30.67% increase when CQDs, as low as 0.1 wt%, are incorporated into the ternary polymer film. This effective improvement is related to the Coulomb blockade effect and trap effect, which will be discussed later. The Weibull distribution is utilized to analyse the characteristic breakdown strength (EBD), under which the films have an 63.2% chance of failure. As illustrated in Fig. 4a and b, the EBD first increases from 265.03 kV mm^{-1} to 322.01 kV mm^{-1} then declines to 264.10 kV mm^{-1} with the addition of CQDs. Here, the characteristic E_b reaches the maximum at 0.1 wt% CQD loading.

Characterization of electric energy storage and energy efficiency

The U_d and energy efficiency are calculated through integrating the P–E loops, whose results are illustrated in Fig. 5. Among all the nanocomposite films, the one with CQD content of 0.1 wt% presents the highest U_d of 6.8 J cm^{-3}, while that of the pristine ternary polymer film is only 4.8 J cm^{-3}. Besides, this nanocomposite film possesses higher energy efficiency up to 68.0% under the electric field of 160 kV mm^{-1}. That is, the U_d and the energy efficiency at 160 kV mm^{-1} are improved by 41.7% and 21.4%, respectively, for the CQD addition as low as 0.1 wt%. Additionally, the energy efficiency shows two turning points in Fig. 5b. The first is associated with the field-induced depolarization, meaning the dipoles can respond to the applied electric field.[43] On the other hand, the ferroelectric domains can interact with each other and the coupling among them can become stronger when the electric field increases to a certain extent.[46] As a result, it is difficult for dipoles to switch back to the equilibrium state, hampering the energy efficiency. In addition, the space charges accumulated on the interfaces can lead to severe conductivity loss.[47] Notably, the U_d of the nanocomposite films are hardly distinguishable from each other, which will be discussed afterwards.

Discussion

To understand the effect of CQDs on the breakdown behaviour of the nanocomposite films, DSC is utilized first. As shown in Fig. 6a, the melting point is around 132 °C, corresponding to that of the ternary polymer. It has been found that the crystallinity first reaches the apex at 0.1 wt% CQD loading then starts to decrease with increasing the filler content. It is speculated that the hydrogen bonds provided by abundant oxygenous

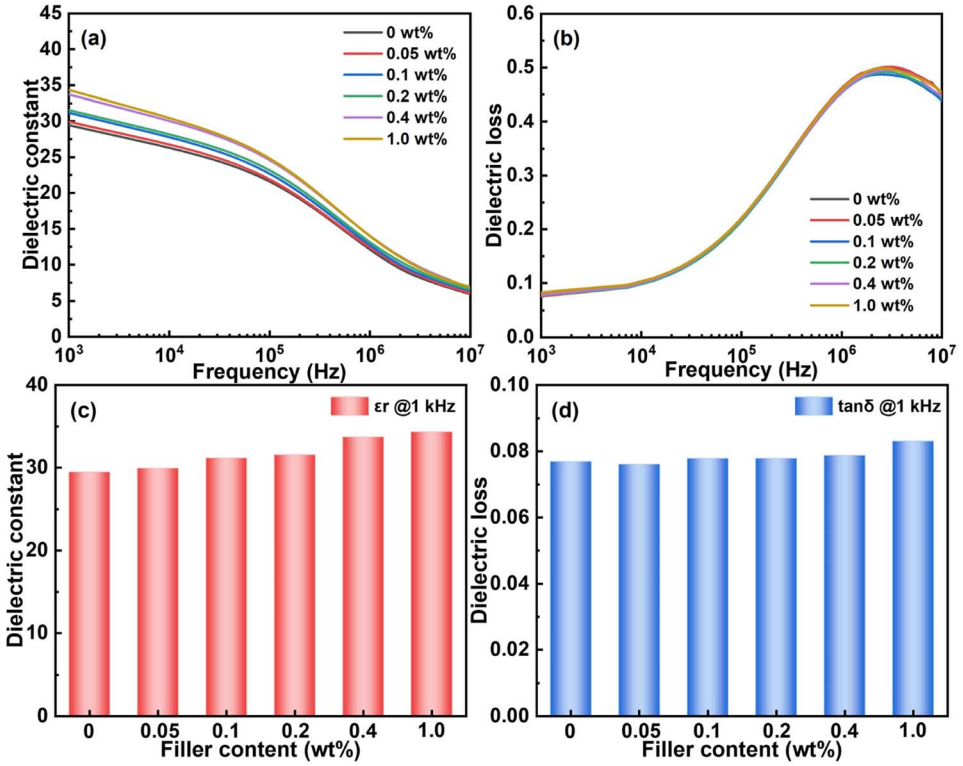

Fig. 3 (a) Dielectric constant. (b) Dielectric loss as a function of frequency. (c) The dielectric constant. (d) Dielectric loss at 1 kHz of pristine ternary polymer thin film and CQDs/P(VDF-TrFE-CTFE) nanocomposites.

functional groups on the CQDs surface are beneficial for polymer chains to align in order and for crystallinity to increase. Note that the sample with CQDs of 0.1 wt% also presents the maximal E_b. To our knowledge, a higher crystallinity is favourable for the improvement of the E_b due to the generated interfaces and extended tree-path brought about by more crystallites.[44,48] On the one hand, polymer chains pack more densely and the free volume is declined in the crystallized area, resulting in a local higher breakdown strength. On the other hand, the electric stress develops along the interface between the crystallites and the polymer matrix when it hits the interface, which is favourable for diverging and weakening the electric stress and then for extending the growth of the electric tree-path. In addition, the crystallites can generate a depolarization electric field and reduce the local field, resulting in a decreased polarization to some extent and a higher electric field endurance.[49] As a result, the sample with a higher crystallinity possesses better energy storage properties.

For another perspective, UV-vis absorption is employed. The band gap energy (E_g) can be estimated by using eqn (2). The UV-

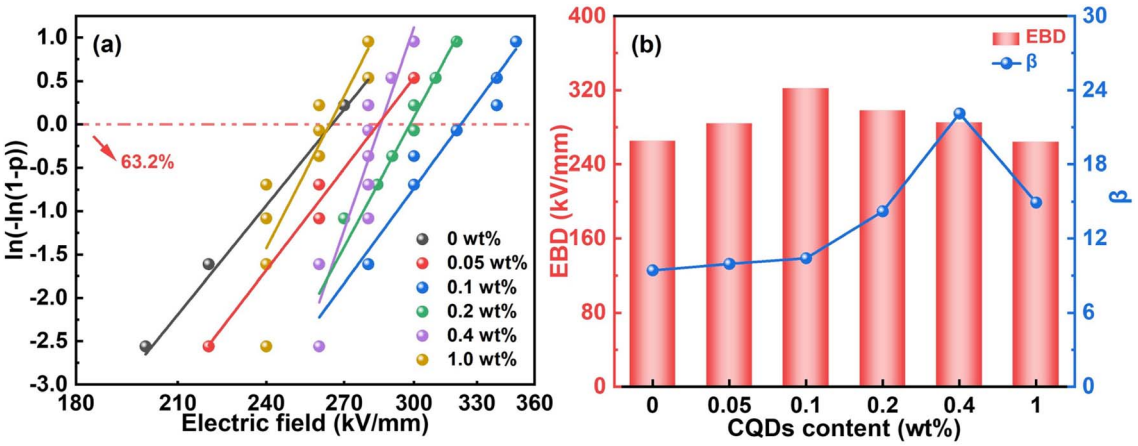

Fig. 4 (a) The Weibull distribution. (b) The corresponding EBD and shape parameters of the samples with different CQD loadings.

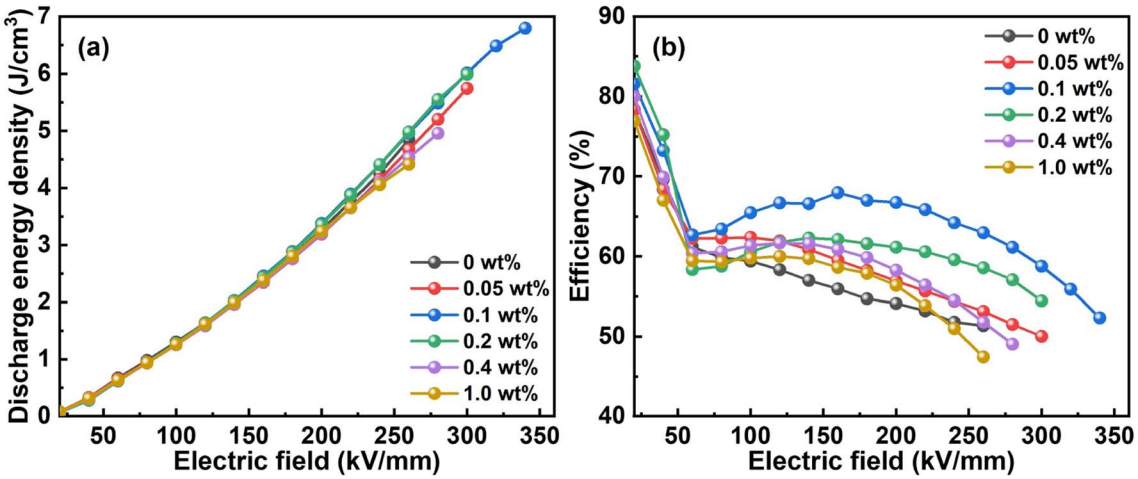

Fig. 5 (a) The discharge energy density and (b) energy efficiency of the samples with different CQDs content.

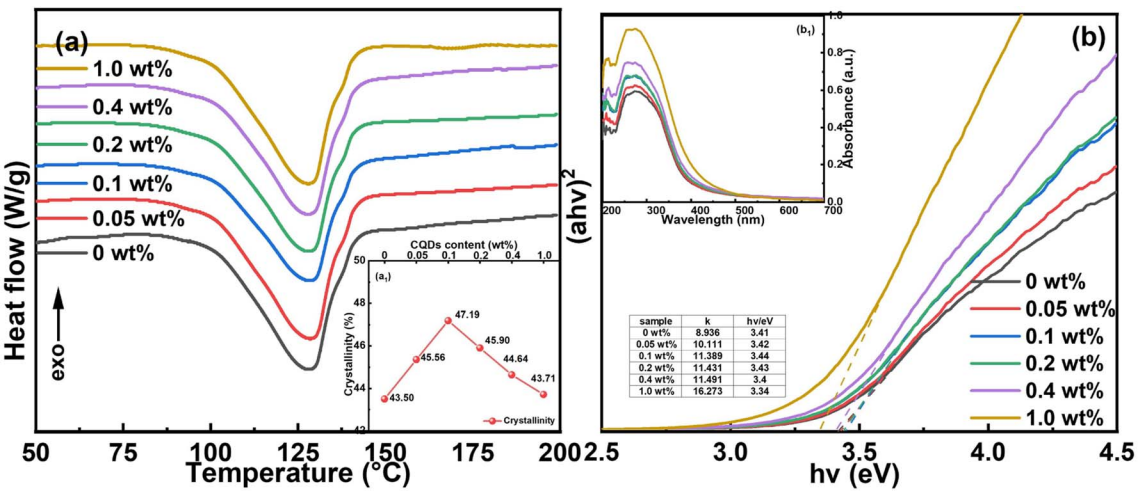

Fig. 6 (a) The DSC curves. (b) The Tauc plot. (a_1) The crystallinity. (b_1) The UV-vis absorption spectra of the samples with different CQD content.

vis absorption spectra and the Tauc plot are shown in Fig. 6b_1 and b, respectively. Notably, the A of the y axis of Fig. 6b is different from the one in eqn (2) due to mathematical analysis. By drawing the tangent line at the steepest position of the curve, the E_g can be found at the intersection of the tangent line with the horizontal axis. The E_g first increases to the peak value at 0.1 wt% CQD loading and then starts to decrease, though the variation is relatively small. Intriguingly, the changing trend here corresponds well with the enhancement of the E_b. By incorporating CQDs, impurity energy level and traps can be introduced, which is favourable for establishing the energy barrier and reducing the charge carriers. Besides, CQDs can help prevent carriers from hopping due to the Coulomb blockade effect by restricting carriers in the deep traps.[37,50] According to Tanaka's multi-layer interface model for dielectric nanocomposites, there are bonded, bound, and loose layers, three types of interface layers, in the interface area, where the chain mobility increases successively. Deep traps can be formed in the bound layer at the interface, which are capable of capturing electrons and preventing them from moving.[39] Therefore, the total concentration of charge carriers can be decreased with decreased leakage current density shown in Fig. S2a (ESI†). In this instance, the possibility for dielectric failure goes down accordingly. Moreover, it has been reported that the influence of the interface will become dominant when the filler size is small enough.[51] Hence, the interface effect brought about by CQDs has played a significant role in improving the E_b of the nanocomposites. Nevertheless, the electron clouds will overlap and more space charges accumulate when the CQD content is over a certain value, leading to a nonuniform local electric field.[52] Moreover, shallow traps in the loose layer at the interface can improve the charge carrier mobility because the electrons trapped by them are more prone to detrap.[39,53,54] Under these conditions, the conductivity loss will emerge and the traps can no longer restrict free carriers. Therefore, the E_b of the nanocomposite film at 1.0 wt% CQD loading is reduced to values close to the initial values.

To further understand the energy storage behaviour of the nanocomposite films, the polarization curves are studied. As illustrated in Fig. 7a, the pristine ternary polymer film reaches

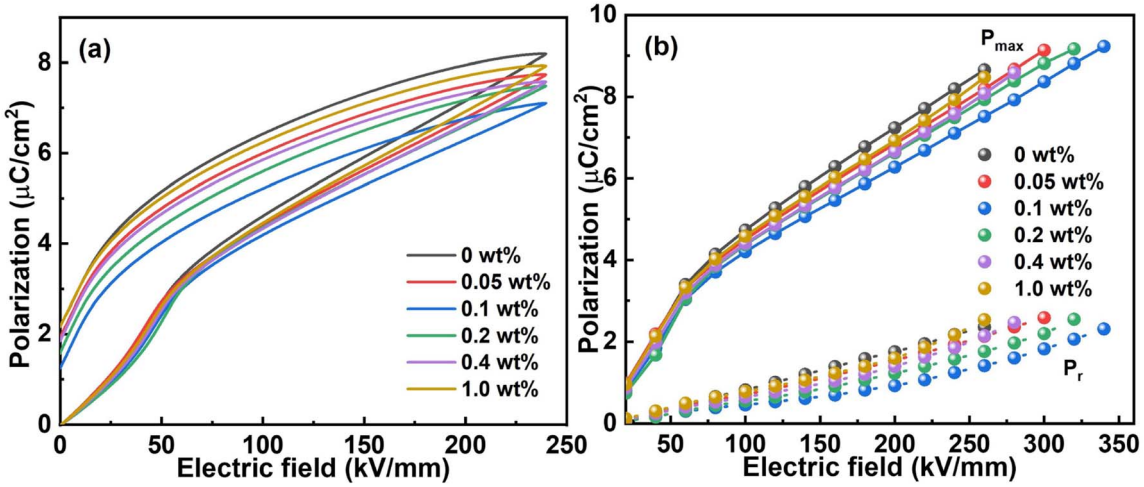

Fig. 7 (a) The P–E loops at 240 kV mm^{-1} and (b) the maximum polarization and remanent polarization at different electric fields of the samples with different CQD content.

the high maximal polarization (P_{max}) quickly due to its premature saturation while a higher remanent polarization (P_r) is retained. Summarizing the P_{max} and P_r with electric field increment of 20 kV mm^{-1}, the differences become clearer in Fig. 7b. It is apparent that the slope belonging to the sample with CQD content of 0.1 wt% is the lowest, which means a valid delay for polarization saturation. According to the P–E curve, a larger integrated area and U_d can be obtained with a delayed polarization. The reason for this phenomenon lies in the O–H···F hydrogen bonds formed at the interfaces due to the strong polymer/filler interaction.[20,47] Because of the hydrogen bonds, the energy barrier for dipoles to respond to the electric field becomes higher, which also explains the inferior polarization and less remanent polarization.[27,55] On the other hand, the

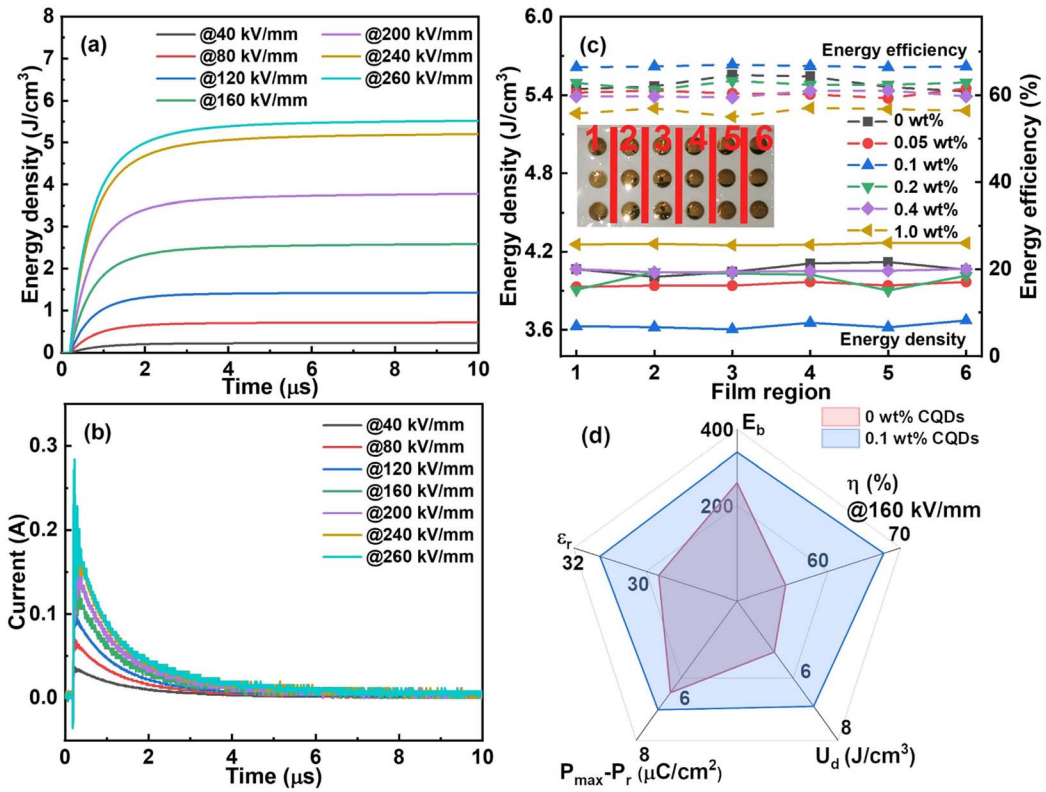

Fig. 8 (a) The W_d as a function of time and (b) pulsed overdamped discharge behaviour of the sample with CQD content of 0.1 wt% at various electric fields. (c) The film stability at 160 kV mm^{-1} of the samples with different CQD content and (d) the comparison between the pristine polymer film and the sample with CQD content of 0.1 wt%.

depolarization electric field generated by crystallites also plays a vital role in diminishing the local field and postponing the polarization saturation. Usually, the larger the integrated area in the *P*–*E* curve, the higher the energy density. However, there is seldom any difference among those samples as mentioned before. The U_d depends on the discharge curve which is associated with both P_{max} and P_r. Take the sample at 1.0 wt% CQD loading for instance: the P_{max} is higher than that of the sample at 0.1 wt% CQD loading while the P_r is higher as well, leading to a very small variation in the calculated U_d. On the other hand, the total energy density of the sample with CQD content of 1.0 wt% is higher absolutely because it is mainly depending on the P_{max}. For this instance, the efficiency of the sample with CQD content of 0.1 wt% is much more satisfactory without a doubt.

For dielectric capacitors, the charge–discharge property is one of the most important indexes to assess whether they can be put into practical applications or not. The W_d and the over-damped current *versus* time curves of the sample with CQD content of 0.1 wt% are shown in Fig. 8a and b. The energy is released rapidly as well as stably and the W_d is up to 5.5 J cm^{-3} at the electric field of 260 kV mm^{-1}. Meanwhile, the discharge current increases gradually with higher electric field. To verify the stability of the nanocomposite films, they are divided into 6 regions factitiously where several points are measured to calculate the average energy density. The results are summarized in Fig. 8c. The 0.1 wt% CQD nanocomposite presents a better cycling stability than the pristine polymer as shown in Fig. S2b (ESI†). Through the comprehensive consideration of the dielectric properties of all the nanocomposite films, the sample at 0.1 wt% CQD loading is thought to be the best performing nanocomposite film with ultralow addition of CQD filler. The comparison between the pristine polymer film and the greatest one is summed up in Fig. 8d. The property comparisons with similar material systems are provided in Table S1 (ESI†).

Conclusions

P(VDF-TrFE-CTFE) added ultra-low CQD filler content nanocomposite films are prepared *via* solution-casting. The best performing one among all the samples is the nanocomposite film with 0.1 wt% CQD loading. The dielectric properties have been improved effectively, especially the breakdown strength. The dielectric constant increases gradually with the addition of CQDs, reaching 34.6 with the CQD content of 1.0 wt%. The E_b has been enhanced 30.7%, as high as 340 kV mm^{-1}. The origin is that depolarization electric field can be generated in the crystallites of the nanocomposites, weakening the local field. Furthermore, CQDs hamper carriers from hopping *via* the Coulomb blockade effect. Consequently, the maximal U_d is up to 6.8 J cm^{-3} which presents a 41.7% increase compared to the pristine ternary polymer film.

It is obvious that the ultralow amount of filler addition facilitates the improvement of the dielectric properties, however, there is still a limitation for practical application. More improvement methods suitable for the P(VDF-TrFE-CTFE) polymer should be conducted in the future.

Experimental

Raw materials

All NaOH, 40% acetaldehyde and HCl are purchased from Sinopharm Chemical Reagent Beijing Co., Ltd. Poly(vinylidenefluoride-trifluoroethylene-chlorotrifluoroethylene) (P(VDF-TrFE-CTFE)) powder is purchased from Polyk Technologies, China; *N*,*N*-dimethylformamide (DMF, ≥99.5%) is purchased from Sinopharm, China; CQDs are synthesized by a simple chemical method mentioned in previous work.[40,56]

The synthesis of CQDs

In brief, 60 g NaOH was dissolved in a moderate amount of water and then the solution was added to 200 mL acetaldehyde aqueous solution (40%), followed by stirring vigorously for 2 h and being placed at ambient air, temperature, and pressure. Then the product is separated by centrifugation and washed with 1 M HCl and deionized water successively, followed by drying in a vacuum oven for 12 h.

The preparation of CQDs/P(VDF-TrFE-CTFE) nanocomposite films

CQDs powder with various mass fractions is dispersed in DMF solvent, followed by a 30 minute sonication to obtain a homogeneous light-yellow solution. P(VDF-TrFE-CTFE) powder is dissolved in the above solution under magnetic stirring at 55 ° C for more than 18 h to obtain a clear solution. The final solution is solution-cast in a glass substrate and dried at 70 °C for 48 h to prepare thin nanocomposite films. The thickness of those films is about 12 μm. Finally, the films are coated golden electrodes *via* magnetron sputtering for dielectric properties testing.

Characterization and instrumentation

The transmission electron microscope (TEM, Titan G2 60-300), SEM (TESCAN MIRA3 LMH), laser scanning confocal microscopy (LSCM, Leica TCS SP8, Germany, $\lambda = 538$ nm), and XPS (Kratos AXIS SUPRA+) are employed to characterize the morphology and microstructure of the CQDs and nanocomposite films. DSC (DSC-25, America, heating rate of 10 °C min^{-1} under a nitrogen atmosphere) is utilized to calculate the crystallinity of the nanocomposites with the formula below:[57]

$$\chi_c = \frac{\Delta H_m}{\Delta H_m{}^0} \times 100\% \quad (1)$$

where χ_c is the crystallinity, ΔH_m is the melting enthalpy od the nanocomposites and the $\Delta H_m{}^0$ is the melting enthalpy of the polymer with 100% of crystallinity (42.0 J g^{-1} for the P(VDF-TrFE-CTFE)).[55]

UV-vis absorption (Shimadzu UV-3600i Plus) is employed to analyse the direct E_g of the nanocomposite films by the Tauc plot method. The E_g can be calculated as follows:[58]

$$(\alpha h\nu)^2 = A(h\nu - E_g) \quad (2)$$

where α, h, and ν represent the light absorption index, Planck constant and the frequency, respectively; and A is a constant while E_g is defined before.

An Agilent 4294A LCR meter with frequency ranging from 1 kHz to 10 MHz and TF analyser 3000 ferroelectric polarization tester (aixACT, Germany) were utilized to test the dielectric properties and measure the P–E loops of the nanocomposites, respectively. Afterwards, the discharged energy density and efficiency were calculated. The characteristic E_b of the nanocomposites is analysed *via* the Weibull distribution:[59]

$$P = 1 - \exp[-(E/E_b)]^{\beta} \quad (3)$$

where P, E, E_b, and β represent the cumulative possibility of electric failure, breakdown strength at a 63.2% possibility of cumulative failure, EBD and the shape parameter assessing the scatter degree of data, respectively.

The discharge energy density (W_d) is an important performance index to directly estimate the practicability of dielectric capacitors. The charge–discharge curves are measured through a simple R–C circuit. And the W_d is calculated from the formula below:[60]

$$W_d = \frac{R\int i^2(t)\mathrm{d}t}{V} \quad (4)$$

where R and V represent the inner resistance (10^4 Ω) and the sample volume, respectively.

Author contributions

D. Zhang and H. Luo conceived and supervised the project. G. Zou, X. Ji and H. Hou provided the CQDs. X. Jiang carried out the nanocomposite material preparations and data analysis. H. Xie and Y. Liu: helped in the material characterization. F. Wang and X. Li: conducted the electrical properties testing. All the authors participated in the discussion and preparation of the manuscript.

Conflicts of interest

There are no conflicts to declare.

Acknowledgements

The authors acknowledge the support from the National Natural Science Foundation of China (52172265 and 52002404), Scientific research project of Hunan Provincial Department of Education (21B0009), Excellent Youth Science Foundation of Hunan Province (2022JJ20067), The Science and Technology Innovation Program of Hunan Province (2022RC1074), Central South University Innovation-Driven Research Program (2023CXQD010) and State Key Laboratory of Powder Metallurgy, Central South University, Changsha, China.

References

1 Z. Ran, B. Du, M. Xiao, H. Liu and J. Xing, Dielectric property improvement of polypropylene films doped with POSS for HVDC polymer film capacitors, *IEEE Trans. Dielectr. Electr. Insul.*, 2021, **28**(4), 1308–1316.
2 G. Wang, Z. Lu, Y. Li, L. Li, H. Ji, A. Feteira, D. Zhou, D. Wang, S. Zhang and I. M. Reaney, Electroceramics for high-energy density capacitors: current status and future perspectives, *Chem. Rev.*, 2021, **121**(10), 6124–6172.
3 M. Singh, I. E. Apata, S. Samant, W. Wu, B. V. Tawade, N. Pradhan, D. Raghavan and A. Karim, Nanoscale strategies to enhance the energy storage capacity of polymeric dielectric capacitors: review of recent advances, *Polym. Rev.*, 2021, **62**(2), 211–260.
4 J. H. Bae and S. H. Chang, PVDF-based ferroelectric polymers and dielectric elastomers for sensor and actuator applications: a review, *Funct. Compos. Struct.*, 2022, **1**, 012003.
5 X. Wu, X. Chen, Q. Zhang and D. Q. Tan, Advanced dielectric polymers for energy storage, *Energy Storage Mater.*, 2022, **44**, 29–47.
6 Q. Feng, J. Ping, J. Zhu, J. Pei, L. Huang, D. Zhang, Y. Zhao, S. Zhong and Z. Dang, All-organic dielectrics with high breakdown strength and energy storage density for high-power capacitors, *Macromol. Rapid Commun.*, 2021, **42**(12), e2100116.
7 Y. Zhuang, S. Han, W. Liu, X. Wei and Z. Xu, An interdigital electrode type sensor based on P(VDF-TrFE) nanofibers, *J. Alloys Compd.*, 2020, **831**, 154657.
8 Y. Lu, Y. Jiang, Z. Lou, R. Shi, D. Chen and G. Shen, Wearable supercapacitor self-charged by P(VDF-TrFE) piezoelectric separator, *Prog. Nat. Sci.: Mater. Int.*, 2020, **30**(2), 174–179.
9 J. Qiu, Q. Gu, Y. Sha, Y. Huang, M. Zhang and Z. Luo, Preparation and application of dielectric polymers with high permittivity and low energy loss: a mini review, *J. Appl. Polym. Sci.*, 2022, **139**(24), 52367.
10 H. Chen, Z. Pan, W. Wang, Y. Chen, S. Xing, Y. Cheng, X. Ding, J. Liu, J. Zhai and J. Yu, Ultrahigh discharge efficiency and improved energy density in polymer-based nanocomposite for high-temperature capacitors application, *Compos. Part A: Appl. Sci. Manuf.*, 2021, **142**, 106266.
11 J. S. Ho and S. G. Greenbaum, Polymer capacitor dielectrics for high temperature applications, *ACS Appl. Mater. Interfaces*, 2018, **10**(35), 29189–29218.
12 T. Zhang, X. Chen, Y. Thakur, B. Lu, Q. Zhang, J. Runt and Q. Zhang, A highly scalable dielectric metamaterial with superior capacitor performance over a broad temperature, *Sci. Adv.*, 2020, **6**(4), eaax6622.
13 Y. Zhu, P. Jiang and X. Huang, Poly(vinylidene fluoride) terpolymer and poly(methyl methacrylate) composite films with superior energy storage performance for electrostatic capacitor application, *Compos. Sci. Technol.*, 2019, **179**, 115–124.
14 J. Lu, B. Zhu, X. Zhang and X. Wang, Dielectric strength structure-activity relationship of BOPP film for high energy density pulse capacitor, *IEEE Trans. Plasma Sci.*, 2019, **47**(9), 4342–4349.
15 L. Lu, W. Ding, J. Liu and B. Yang, Flexible PVDF based piezoelectric nanogenerators, *Nano Energy*, 2020, **78**, 105251.

16 A. Salimi and A. Yousefi, FTIR studies of β-phase crystal formation in stretched PVDF films, *Polym. Test.*, 2003, **22**(6), 699–704.
17 Y. j. Cho, J. Jeong, M. Choi, G. Baek, S. Park, H. Choi, S. Ahn, S. Cha, T. Kim and D. Kang, $BaTiO_3$@ PVDF-TrFE nanocomposites with efficient orientation prepared *via* phase separation nano-coating method for piezoelectric performance improvement and application to 3D-PENG, *Chem. Eng. J.*, 2022, **427**, 131030.
18 S. Barrau, A. Ferri, A. Da Costa, J. Defebvin, S. Leroy, R. Desfeux and J.-M. Lefebvre, Nanoscale investigations of α-and γ-crystal phases in PVDF-based nanocomposites, *ACS Appl. Mater. Interfaces*, 2018, **10**(15), 13092–13099.
19 L. Jin, S. Ma, W. Deng, C. Yan, T. Yang, X. Chu, G. Tian, D. Xiong, J. Lu and W. Yang, Polarization-free high-crystallization β-PVDF piezoelectric nanogenerator toward self-powered 3D acceleration sensor, *Nano Energy*, 2018, **50**, 632–638.
20 C. Zhao, Y. Hong, X. Chu, Y. Dong, Z. Hu, X. Sun and S. Yan, Enhanced ferroelectric properties of P(VDF-TrFE) thin film on single layer graphene simply adjusted by crystallization condition, *Mater. Today Energy*, 2021, **20**, 100678.
21 M. R. Gadinski, Q. Li, G. Zhang, X. Zhang and Q. Wang, Understanding of relaxor ferroelectric behavior of poly(vinylidene fluoride–trifluoroethylene–chlorotrifluoroethylene)terpolymers, *Macromolecules*, 2015, **48**(8), 2731–2739.
22 F. Bargain, D. Thuau, G. Hadziioannou, F. Domingues Dos Santos and S. Tencé-Girault, Phase diagram of poly(VDF-ter-TrFE-ter-CTFE)copolymers: relationship between crystalline structure and material properties, *Polymer*, 2021, **213**, 123203.
23 Y. Huang, T. Gu, G. Rui, P. a. Shi, W. Fu, L. Chen, X. Liu, J. Zeng, B. Kang, Z. Yan, F. J. Stadler, L. Zhu, F. Kang and Y. He, A relaxor ferroelectric polymer with an ultrahigh dielectric constant largely promotes the dissociation of lithium salts to achieve high ionic conductivity, *Energy Environ. Sci.*, 2021, **14**(11), 6021–6029.
24 Q. Feng, S. Zhong, J. Pei, Y. Zhao, D. Zhang, D. Liu, Y. Zhang and Z. Dang, Recent progress and future prospects on all-organic polymer dielectrics for energy storage capacitors, *Chem. Rev.*, 2022, **122**(3), 3820–3878.
25 B. Chu, X. Zhou, K. Ren, B. Neese, M. Lin, Q. Wang, F. Bauer and Q. M. Zhang, A dielectric polymer with high electric energy density and fast discharge speed, *Science*, 2006, **313**(5785), 334–336.
26 J. Dong, X. Deng, Y. Niu, Z. Pan and H. Wang, Research progress of polymer based dielectrics for high-temperature capacitor energy storage, *Acta Phys. Sin.*, 2020, **69**(21), 217701.
27 M. Zhang, S. Tan, J. Xiong, C. Chen, Y. Zhang, X. Wei and Z. Zhang, Tailoring dielectric and energy storage performance of PVDF-based relaxor ferroelectrics with hydrogen bonds, *ACS Appl. Energy Mater.*, 2021, **4**(8), 8454–8464.
28 X. Li, Y. Yang, Y. Wang, S. Pang, J. Shi, X. Ma and K. Zhu, Enhanced energy storage density of all-organic fluoropolymer composite dielectric *via* introducing crosslinked structure, *RSC Adv.*, 2021, **11**(25), 15177–15183.
29 Y. Shang, Y. Feng, C. Li, C. Zhang, T. Zhang, Y. Zhang, Y. Zhang, C. Song and Q. Chi, Energy storage properties of P(VDF-TrFE-CTFE)-based composite dielectrics with uniform and gradient-doped boron nitride nanosheets, *IET Nanodielectr.*, 2021, **5**(1), 50–61.
30 L. Li, J. Cheng, Y. Cheng, T. Han, Y. Liu, Y. Zhou, G. Zhao, Y. Zhao, C. Xiong, L. Dong and Q. Wang, Significant improvements in dielectric constant and energy density of ferroelectric polymer nanocomposites enabled by ultralow contents of nanofillers, *Adv. Mater.*, 2021, **33**(35), e2102392.
31 R. Guo, L. Li, B. Wang, Y. Xiang, G. Zou, Y. Zhu, H. Hou and X. Ji, Functionalized carbon dots for advanced batteries, *Energy Storage Mater.*, 2021, **37**, 8–39.
32 T. C. Wareing, P. Gentile and A. N. Phan, Biomass-based carbon dots: current development and future perspectives, *ACS Nano*, 2021, **15**(10), 15471–15501.
33 B. Domingo-Tafalla, E. Martinez-Ferrero, F. Franco and E. Palomares-Gil, Applications of carbon dots for the photocatalytic and electrocatalytic reduction of CO_2, *Molecules*, 2022, **27**(3), 1081.
34 M. Ji, Y. Liu, J. Di, R. Chen, Z. Chen, J. Xia and H. Li, N-CQDs accelerating surface charge transfer of $Bi_4O_5I_2$ hollow nanotubes with broad spectrum photocatalytic activity, *Appl. Catal., B*, 2018, **237**, 1033–1043.
35 V. A. e. Burdov, The quantum control of electron states in a double quantum dot under coulomb blocking conditions, *J. Exp. Theor. Phys.*, 2002, **76**(1), 21–25.
36 A. Donarini, G. Begemann and M. Grifoni, Interference effects in the Coulomb blockade regime: current blocking and spin preparation in symmetric nanojunctions, *Phys. Rev. B: Condens. Matter Mater. Phys.*, 2010, **82**(12), 125451.
37 L. F. Schelp, A. Fert, F. Fettar, P. Holody, S. F. Lee, J. L. Maurice, F. Petroff and A. Vaures, Spin-dependent tunneling with Coulomb blockade, *Phys. Rev. B: Condens. Matter Mater. Phys.*, 1997, **56**(10), R5747–R5750.
38 T. Tanaka, M. Kozako, N. Fuse and Y. Ohki, Proposal of a multi-core model for polymer nanocomposite dielectrics, *IEEE Trans. Dielectr. Electr. Insul.*, 2005, **12**(4), 669–681.
39 Y. Zhou, J. Hu, B. Dang and J. He, Titanium oxide nanoparticle increases shallow traps to suppress space charge accumulation in polypropylene dielectrics, *RSC Adv.*, 2016, **6**(54), 48720–48727.
40 H. Hou, L. Shao, Y. Zhang, G. Zou, J. Chen and X. Ji, Large-area carbon nanosheets doped with phosphorus: a high-performance anode material for sodium-ion batteries, *Adv. Sci.*, 2017, **4**(1), 1600243.
41 P. Ge, H. Hou, X. Cao, S. j. Li, G. Zhao, T. Guo, C. Wang and X. Ji, Multidimensional evolution of carbon structures underpinned by temperature-induced intermediate of chloride for sodium-ion batteries, *Adv. Sci.*, 2018, **5**(6), 1800080.
42 L. Zhu, Exploring strategies for high dielectric constant and low loss polymer dielectrics, *J. Phys. Chem. Lett.*, 2014, **5**(21), 3677–3687.

43 M. Yuan, B. Li, S. Zhang, R. Rajagopalan and M. T. Lanagan, High-field dielectric properties of oriented poly(vinylidene fluoride-co-hexafluoropropylene): structure–dielectric property relationship and implications for energy storage applications, *ACS Appl. Polym. Mater.*, 2020, **2**(3), 1356–1368.

44 Y. Guo, N. Meng, Y. Zhang, J. Xu, E. Pawlikowska, C. y. Wu, M. Szafran and F. Gao, Characterization and performance of plate-like $Ba_{0.6}Sr_{0.4}TiO_3$/poly(vinylidene fluoride-trifluoroethylene-chlorotrifluoroethylene) composites with high permittivity and low loss, *Polymer*, 2020, **203**, 122777.

45 J. Wang, S. Liu, C. Chen, H. Hao and J. Zhai, Interface modification and energy storage properties of barium titanate-based/polyvinylidene fluoride composite, *Acta Phys. Sin.*, 2020, **69**(21), 217702.

46 N. Meng, X. Zhu, R. Mao, M. J. Reece and E. Bilotti, Nanoscale interfacial electroactivity in PVDF/PVDF-TrFE blended films with enhanced dielectric and ferroelectric properties, *J. Mater. Chem. C*, 2017, **5**(13), 3296–3305.

47 Y. Feng, Q. Deng, C. Peng, J. Hu, Y. Li, Q. Wu and Z. Xu, An ultrahigh discharged energy density achieved in an inhomogeneous PVDF dielectric composite filled with 2D MXene nanosheets *via* interface engineering, *J. Mater. Chem. C*, 2018, **6**(48), 13283–13292.

48 T. Soulestin, V. Ladmiral, F. D. Dos Santos and B. Améduri, Vinylidene fluoride- and trifluoroethylene-containing fluorinated electroactive copolymers. How does chemistry impact properties?, *Prog. Polym. Sci.*, 2017, **72**, 16–60.

49 F. Guan, J. Wang, L. Yang, J.-K. Tseng, K. Han, Q. Wang and L. Zhu, Confinement-induced high-field antiferroelectric-like behavior in a poly(vinylidene fluoride-co-trifluoroethylene-co-chlorotrifluoroethylene)-graft-polystyrene graft copolymer, *Macromolecules*, 2011, **44**(7), 2190–2199.

50 S. Li, J. Dong, Y. Niu, L. Li, F. Wang, R. Hu, J. Cheng, L. Sun, Z. Pan, X. Xu and H. Wang, Enhanced high-temperature energy storage properties of polymer composites by interlayered metal nanodots, *J. Mater. Chem. A*, 2022, **10**(36), 18773–18781.

51 T. J. Lewis, Interfaces: nanometric dielectrics, *J. Phys. D*, 2005, **38**(2), 202–212.

52 Y. Thakur, T. Zhang, C. Iacob, T. Yang, J. Bernholc, L. Chen, J. Runt and Q. Zhang, Enhancement of the dielectric response in polymer nanocomposites with low dielectric constant fillers, *Nanoscale*, 2017, **9**(31), 10992–10997.

53 R. Qiao, C. Wang, S. Chen, G. He, Z. Liu, H. Luo and D. Zhang, High-temperature dielectric polymers with high breakdown strength and energy density *via* constructing the electron traps in blends, *Compos. Part A: Appl. Sci. Manuf.*, 2022, **152**, 106679.

54 S. Wang, Z. Luo, J. Liang, J. Hu, N. Jiang, J. He and Q. Li, Polymer nanocomposite dielectrics: understanding the matrix/particle interface, *ACS Nano*, 2022, **16**(9), 13612–13656.

55 R. Wang, H. Xu, S. Cheng, J. Liang, B. Gou, J. Zhou, J. Fu, C. Xie, J. He and Q. Li, Ultrahigh-energy-density dielectric materials from ferroelectric polymer/glucose all-organic composites with a cross-linking network of hydrogen bonds, *Energy Storage Mater.*, 2022, **49**, 339–347.

56 W. Hong, Y. Zhang, L. Yang, Y. Tian, P. Ge, J. Hu, W. Wei, G. Zou, H. Hou and X. Ji, Carbon quantum dot micelles tailored hollow carbon anode for fast potassium and sodium storage, *Nano Energy*, 2019, **65**, 104038.

57 T. Soulestin, P. Marcelino Dos Santos Filho, V. Ladmiral, C. Totée, G. Silly, T. Lannuzel, F. Domingues Dos Santos and B. Ameduri, Influence of trans-1,3,3,3-tetrafluoropropene on the structure–properties relationship of VDF- and TrFE-based terpolymers, *Macromolecules*, 2017, **50**(2), 503–514.

58 S. Mandal, A. C. Reber, M. c. Qian, P. S. Weiss, S. N. Khanna and A. Sen, Controlling the band gap energy of cluster-assembled materials, *Acc. Chem. Res.*, 2013, **46**(11), 2385–2395.

59 L. Sun, Z. Shi, B. He, H. Wang, S. Liu, M. Huang, J. Shi, D. Dastan and H. Wang, Asymmetric trilayer all-polymer dielectric composites with simultaneous high efficiency and high energy density: a novel design targeting advanced energy storage capacitors, *Adv. Funct. Mater.*, 2021, **31**(35), 2100280.

60 X. Zhao, C. Li, J. k. Liu, Y. Ding, W. Bai, P. Zheng, P. Li, J. Zhang and J. Zhai, $(Bi_{0.5}Na_{0.5})TiO_3$-based relaxor ferroelectrics with simultaneous high energy storage properties and remarkable charge-discharge performances under low working electric fields for dielectric capacitor applications, *Ceram. Int.*, 2021, **47**(18), 25800–25809.